ACS NANO
Cite This: ACS Nano 2018, 12, 10529−10536
www.acsnano.org

ARTICLE

# Enhancement of Out-of-Plane Charge Transport in a Vertically Stacked Two-Dimensional Heterostructure Using Point Defects

Yanran Liu,[†] Zhibin Gao,[‡,§,⊥] Yang Tan,*[,†] and Feng Chen*[,†]

[†]School of Physics, State Key Laboratory of Crystal Materials, Shandong University, Jinan, Shandong 250100, China
[‡]Center for Phononics and Thermal Energy Science, [§]China-EU Joint Center for Nanophononics, and [⊥]Shanghai Key Laboratory of Special Artificial Microstructure Materials and Technology, School of Physics Science and Engineering, Tongji University, Shanghai 200092, China

Supporting Information

**ABSTRACT:** **Point defects in 2D materials block in-plane charge transport, which incurs negative effects on the photoresponse of 2D monolayer materials. In contrast to in-plane charge transport, we show that out-of-plane charge transport in 2D materials can be enhanced through controllable formation of point defects, thus enhancing the photoresponse of a vertical heterostructure. Graphene and $WSe_2$ monolayers were stacked together to construct a vertical heterostructure (W/G). Se point defects were artificially formed on the top atomic layer of $WSe_2$ with controllable density *via* Ga ion irradiation. The interlayer charge transport in the W/G heterostructure was detected with femtosecond optical probe−pump measurements and photoelectric detection. Our experiments show that point defects can be used to provide higher transfer rate for out-of-plane charge transport and more electronic states for photoexcitation, leading to enhanced photoinduced interlayer charge transfer from $WSe_2$ to graphene. Based on this feature, a photodetector based on W/G modified by point defects is proposed and implemented, exhibiting a fast photoresponsivity (~0.6 ms) (2 orders of magnitude larger than the photoresponse in pristine W/G). This work demonstrates that out-of-plane charge transport is enhanced by the presence of point defects and illustrates an efficient method to optimize the performance of photoelectric devices based on vertical heterostructures.**

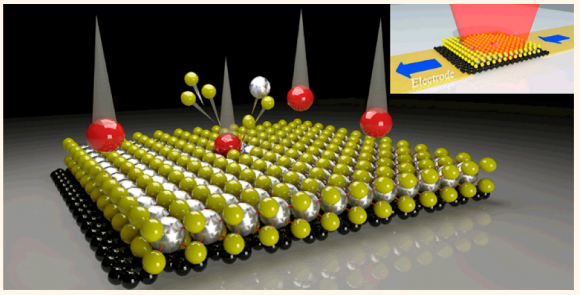


**KEYWORDS:** *TMDCs, localized states, heterostructure, photodetector, ion irradiation*

Vertical two-dimensional (2D) heterostructures can be assembled by stacking isolated atomic planes layer-by-layer in an arbitrary sequence.[1−3] At the interface between stacked atomic layers, interlayer coupling modifies the electronic properties of the isolated 2D materials[4,5] and creates material systems with fascinating physical properties.[6] Early studies suggest that the optoelectronic properties of 2D materials are dramatically enriched due to interlayer coupling. As functionalities of vertical heterostructures are dominated by interlayer coupling between adjacent layers,[7−9] there is a continuous interest to explore ways to promote interlayer interactions in vertical heterostructures.

After graphene,[10] 2D transition metal dichalcogenides (TMDCs) have received great attention due to their direct band gap features. These materials are recognized as potential building blocks for optoelectronic nanodevices.[11] Recently, there has been intense interest in $WSe_2$ monolayers owing to their high specific detectivity, high optical gain, and excellent ON/OFF current ratio. Wee's group provided a deep understanding of the effect of metal contacts on the performance of TMDC phototransistors.[12,13] They found that high Schottky contact $WSe_2$ phototransistors display a fast response time (less than 23 ms).[14] High photoresponsivity and fast photoresponse make $WSe_2$ monolayers an excellent photoelectric material for nanodevices.

However, $WSe_2$ monolayers have relatively low formation energy in comparison to that of graphene, and point defects are easily found in $WSe_2$ monolayers.[15,16] As previously reported, point defects hamper charge transfer in the plane of TMDCs.[17−19] Electrons near a point defect are localized

Received: August 26, 2018
Accepted: September 19, 2018
Published: September 19, 2018






DOI: 10.1021/acsnano.8b06503
ACS Nano 2018, 12, 10529−10536

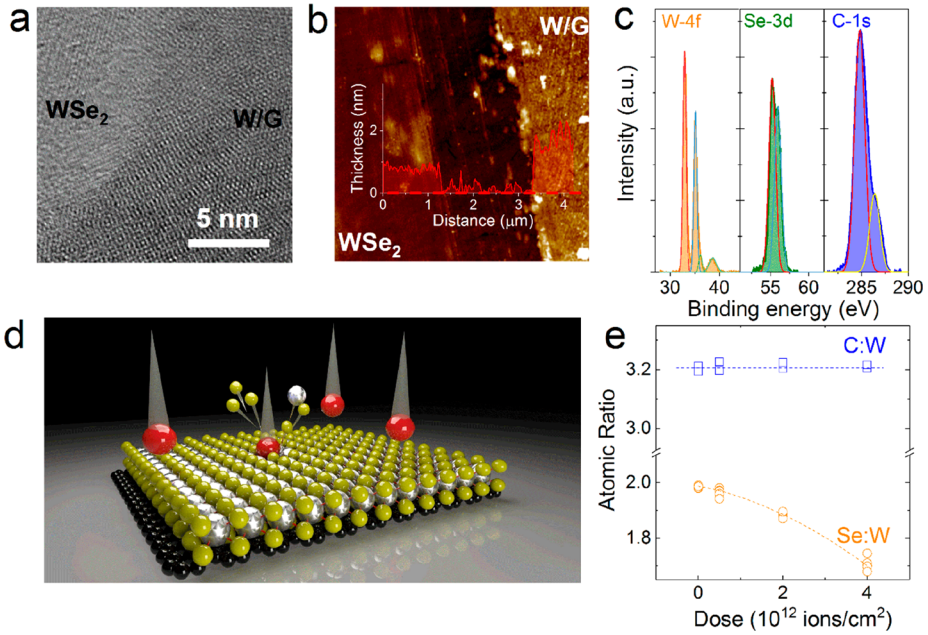


**Figure 1. (a) HRTEM image, (b) AFM image, and (c) EDX image of the as-prepared W/G heterostructure. (d) Schematic diagram of the Ga ion irradiation. (e) Evolution of the atomic ratio as a function of the dose of the incident Ga ion beam.**

with weak dispersion, and charge transport is dominated by hopping *via* these localized gap states, resulting in a transfer rate lower than what would be expected from theoretical calculations. The transfer rate is also lower than the value observed due to native n-type doping. As a result, the in-plane charge transport in the $WSe_2$ is blocked by point defects. Thus, point defects are commonly recognized as a negative factor for in-plane charge transfer. If the out-of-plane charge transfer is not hampered by point defects, $WSe_2$ with defects can still function well in a vertical heterostructure. Therefore, it is interesting to explore the impact of point defects on out-of-plane charge transport in $WSe_2$-based vertical heterostructures.

In this work, we present results showing that point defects in $WSe_2$ monolayers increase the transfer rate and quantity of out-of-plane charge transport. The $WSe_2$ monolayer was coated on the surface of graphene, yielding a vertical heterostructure (W/G). Point defects with controllable density were generated in the $WSe_2$ monolayer *via* Ga ion irradiation, which tunes the density of the Se point defects. Charge transfer between graphene and irradiated $WSe_2$ monolayers was detected by femtosecond (fs) probe−pump spectroscopy and interlayer photocurrent measurements. The fs optical pump−probe measurements indicate that point defects increased the transfer rate of out-of-plane charge transport and the total density of electronic states, leading to enhanced interlayer charge transfer. More direct evidence was observed *via* interlayer photocurrent measurements. Interlayer photocurrent in W/G heterostructures significantly increased when point defects were present. Based on the previous discussion, we used the irradiated W/G heterostructure as a platform to construct a photodetector. We find that point defects increase the enhancement factor by 2 orders of magnitude and expand the optical response from the visible to the near-infrared range (1064 nm). This work shows that point defects enhance out-of-plane charge transfer in TMDCs and demonstrate an efficient method for optimizing vertical heterostructures for photoelectric applications.

Vertical vdW heterostructures (W/G) were constructed by stacking graphene and $WSe_2$ monolayers together. The graphene and $WSe_2$ monolayers were fabricated by chemical vapor deposition (CVD) on an aluminum oxide ($Al_2O_3$) wafer and a copper sheet, respectively. Figure 1a shows a high-resolution transmission electron microscopy (HRTEM) image of W/G, in which there is a boundary between a $WSe_2$ monolayer (with periodic atom arrangement) and W/G (with a Moiré pattern) demonstrating crystallinity of the as-prepared W/G heterostructure. Figure 1b shows atomic force microscope (AFM) topographic data from the W/G heterostructures. The thicknesses of the $WSe_2$ and W/G layers were approximately 1 and 1.5 nm, respectively. The elementary composition of W/G was determined from energy-dispersive X-ray (EDX) measurements, as shown in Figure 1c.

Point defects on the $WSe_2$ monolayer were induced *via* ion irradiation, where ions can sputter surface atoms away from the irradiated material. The as-prepared $WSe_2$ ($S_0$) layer has a stoichiometric ratio of Se/W = 2.002 and C/Se = 3.205, confirming the high crystallinity of the as-prepared W/G heterostructure (Figure 1c). Then, an as-prepared W/G heterostructure with a top $WSe_2$ layer was irradiated with a Ga ion beam and controlled irradiation time ($S_1$ = 2 s; $S_2$ = 4 s, and $S_3$ = 8 s). During the ion irradiation process, the energetic Ga ion impacts the $WSe_2$ monolayer, and Se atoms are sputtered away from the top atomic layer, leaving Se vacancies (Figure 1d). The atomic ratios of Se/W and C/Se were repeatedly determined from XPS measurements. As shown in Figure 1e, the ratio of C/W remained constant after irradiation, and the value of Se/W gradually decreased to 1.99 ($S_1$), 1.98 ($S_2$), and 1.96 ($S_3$). The invariable ratio of C/W indicates the graphene layer remained protected during ion irradiation, and the decreased ratio of Se/W indicates that Se atoms were removed by energetic Ga ions, leaving Se point defects. It should be pointed out that, in the present work, the dose of the Ga ions is relatively low. High-dose Ga ion irradiation result in extended defective/amorphized regions



DOI: 10.1021/acsnano.8b06503
*ACS Nano* 2018, 12, 10529−10536

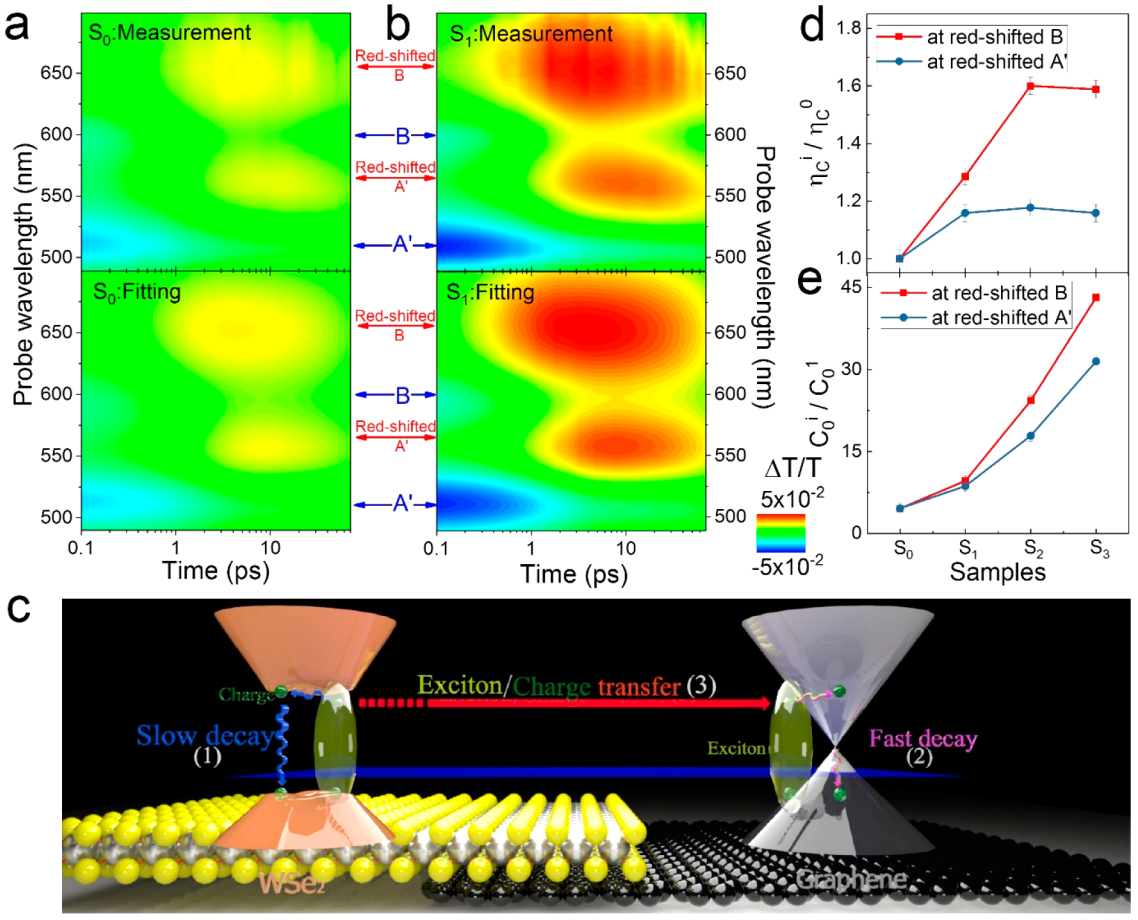


**Figure 2. Contour plots of the $\Delta T/T_0$ spectra of $S_0$ (a) and $S_1$ (b). (c) Schematic diagram showing electronic transitions between graphene and the $WSe_2$ monolayer. The evolution of the transfer rate of (d) the interlayer charge transfers ($\eta_C^i/\eta_C^0$) and (e) the total quantity of the transferred charges ($C_0^i/C_0^0$), corresponding to the red-shifted A′ and B, respectively.**

due to the accumulation of ion-induced damage, which requires further investigation in detail.

## RESULTS

We detected photoexcited charge transport in W/G heterostructures ($S_0$, $S_1$, $S_2$, and $S_3$) using fs optical pump−probe measurements. During the measurement, the W/G heterostructure is excited by a pump light (a 400 nm and 100 fs laser pulse with a peak fluence of 200 $\mu J/cm^2$) and probed by a wide broadband light (450−750 nm). Figures 2a,b and S1 (Supporting Information Part I) show the measured time-resolved different transmission ($\Delta T/T_0$) spectra of the W/G heterostructures. In $\Delta T/T_0$ spectra, we can observe photobleaching (negative signal, $\Delta T/T > 0$) at exciton resonances (A′ and B), as well as a corresponding red-shifted photoinduced absorption peak (positive signal, $\Delta T/T < 0$).[30,31] Photobleaching and the photoinduced absorption are induced by excitons and charges, respectively, and their intensity has a direct relationship with the quantity of photoexcited excitons and charges (Supporting Information Part II).

Under light illumination, three underlying dynamic photoexcitation processes occur in the vertical W/G heterostructure depicted in Figure 2c. (1) In $WSe_2$: light generates excitons ($E$) as the primary photoexcited species.[20−24] Within a characteristic time ($\tau_{WSe_2}$), these excitons dissociate into charges (carrier and hole). Charges ($C$) recombine in the valence band with a long recombination time ($\kappa_{WSe_2}$). This decay process (including dissociation and recombination) lasts more than 50 ps and is labeled "long decay" in Figure 2c. (2) In graphene: The same dynamic photoexcitation process occurs in graphene, except the dissociation ($\tau_{Grap}$) and recombination ($\kappa_{Grap}$) times are much shorter.[25,26] Compared to that of $WSe_2$, the decay processes in graphene are ultrafast (less than 0.5 ps). This process is labeled "fast decay" in Figure 2c. (3) Out-of-plane: Charge and exciton transport occurs between graphene and $WSe_2$.[27,28] As the decay time in graphene is ultrashort, we suspect that charge/exciton transport is unidirectional from $WSe_2$ to graphene, and graphene functions as an additional fast channel for recombination of photogenerated carriers in $WSe_2$. The photoexcitation dynamics in a W/G heterostructure can be expressed with the following equations:[29−31]

$$\frac{dE(t)}{dt} = G(t) - \frac{(1-\eta_E)}{\tau_{WSe}}E(t) - \frac{\eta_E}{\tau_{Grap}}E(t) \quad (1)$$

$$\frac{dC(t)}{dt} = \frac{(1-\eta_E)}{\tau_{WSe}}E(t) - (1-\eta_C)\frac{1}{\kappa_{WSe}}C(t) - \eta_C\frac{1}{\kappa_{Grap}}C(t) \quad (2)$$

$$C_0 = \int \eta_C C(t)dt \quad (3)$$



DOI: 10.1021/acsnano.8b06503
ACS Nano 2018, 12, 10529−10536

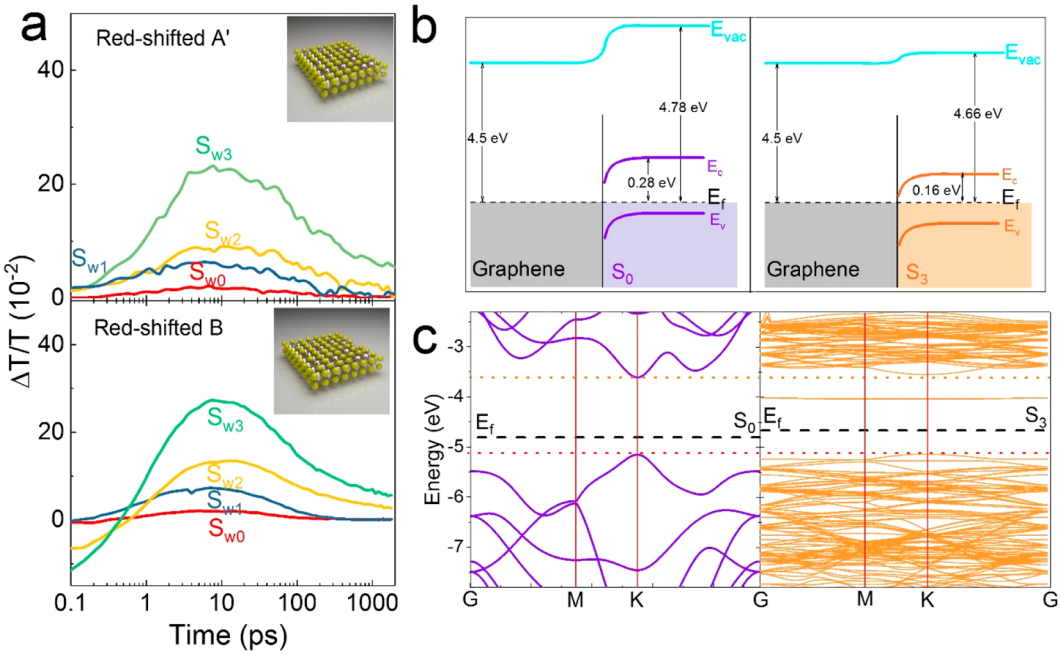


**Figure 3. (a) Measured $\Delta T/T$ spectra of the irradiated $WSe_2$ monolayers at the red-shifted A′ and B. (b) Corresponding energy band diagram of the graphene−$WSe_2$ contact. (c) Calculated electronic structure of $S_0$ and $S_3$.**

where $E$ and $C$ are the time-dependent overall exciton and charge populations in W/G, respectively; $G$ is the exciton generation term; $\eta_E$ and $\eta_C$ are the mobilities of interlayer transport of excitons and charges from $WSe_2$ to graphene, respectively; $C_0$ is the total quantity of out-of-plane charge transport. To simplify the calculation, we suspect that the decay of transferred excitons in graphene is too fast to be considered in eq 2, thus it has been omitted.

To specifically probe the out-of-plane charge transport, we fit the measured $\Delta T/T$ spectra to eqs 1 and 2 to determine the transfer rate ($\eta_C^i$) and quantity ($C_0^i$) of out-of-plane charge transport in $S_0$, $S_1$, $S_2$, and $S_3$ (Supporting Information Part III). Here, $i$ denotes the sample number (0, 1, 2, and 3). The fitted $\Delta T/T$ spectra are displayed in Figures 2a,b and S1, with the coefficient of determination larger than 0.982. Figure 2d,e shows evolutions of $\eta_C^i/\eta_C^0$ and $C_0^i/C_0^0$ corresponding to the red-shifted A′ and B peaks, respectively. Along with the decreasing atomic ratio (Se/W), $\eta_C$ increased by a factor 1.2 for the red-shifted A′ peak (a factor of 1.6 larger than the red-shifted B peak), and $C_0$ increased by a factor 31.5 at the red-shifted A′ peak (a factor 43.2 larger than the red-shifted B peak).

One should note that the variation of $C_0$ is much larger than $\eta_C$. A possible reason is that the total density of electronic states of $WSe_2$ is increased with decreased atomic ratio, which provides more photoexcited charges for out-of-plane transport. To verify this deduction, we detected $\Delta T/T$ spectra of $WSe_2$ monolayers irradiated under the same conditions (Ga ion irradiation and irradiation time of 2, 4, and 8 s, labeled $S_{1w}$, $S_{2w}$, and $S_{3w}$, respectively) for comparison. Figure 3a shows the measured $\Delta T/T$ spectra of the irradiated $WSe_2$ monolayers at the red-shifted A′ and B peaks. Obviously, the peak value for $S_{3w}$ increased by a factor 28 compared with that of the pristine $WSe_2$ monolayer ($S_{0w}$), which confirms that the presence of point defects increases the density of electronic states, leading to the enhancement of $C_0$.

The enhancement of $\eta_C$ can be explained by the Schottky barrier (SB) at the contact of graphene−$WSe_2$. The corresponding energy band diagram of the graphene−$WSe_2$ contact is shown in Figure 3b. As the charge transport is present in the form of the hole transmission in the p-type $WSe_2$, there is a SB in the valence band region. In this case, photoexcited charges cross the SB *via* the thermal excitation, or tunneling at the band edge, or by thermally assisted tunneling (combination of the first two mechanisms). We reconstructed the electronic structure of $S_0$ and $S_3$ by first-principles calculation in Figure 3c. The calculated results suggest that the HOMO (highest occupied molecular orbital) and LUMO (lowest unoccupied molecular orbital) are the same before and after ion irradiation. However, the Fermi surface ($E_F$) of the $WSe_2$ is slightly increased from −4.78 eV ($S_0$) to −4.66 eV ($S_3$). Work functions of the graphene and ITO are −4.5 and −4.85 eV based on literature. The increased $E_F$ reduces the height of the SB at the contact. We suspect the reduced SB is the reason for slightly enhanced $\eta_C$.

Based on the previous discussion, it is easy to conclude that point defects enhance out-of-plane charge transport in the W/G heterostructure. To obtain more direct evidence for this phenomenon, we detected the interlayer photocurrent between adjacent monolayers, based on a vertical W/G photodiode. The side view schematic of the photocurrent is shown in Figure 4a, in which the indium tin oxide glass (ITO/glass) is coated onto the surface of the $WSe_2$. Figure 4b shows the transfer characteristics of the as-prepared W/G ($S_0$) photodiode, which is illuminated by a 532 nm laser with 21 mW of power. Here, the $S_0$ exhibits the nonlinear $I_D-V_D$ curve, indicating SBs at contacts of graphene−$WSe_2$ and $WSe_2$−ITO. The corresponding energy band diagram of the $S_0$ photodiode is shown in Figure 4c. The evolution of the interlayer current in the irradiated samples ($S_1$, $S_2$, and $S_3$) is displayed in Figure 4b. The interlayer current in $S_1$ is almost 2 orders of magnitude larger than the interlayer current in $S_0$. Compared with $S_0$, the interlayer current increased by 3 orders of magnitude in $S_2$ and



DOI: 10.1021/acsnano.8b06503
ACS Nano 2018, 12, 10529−10536

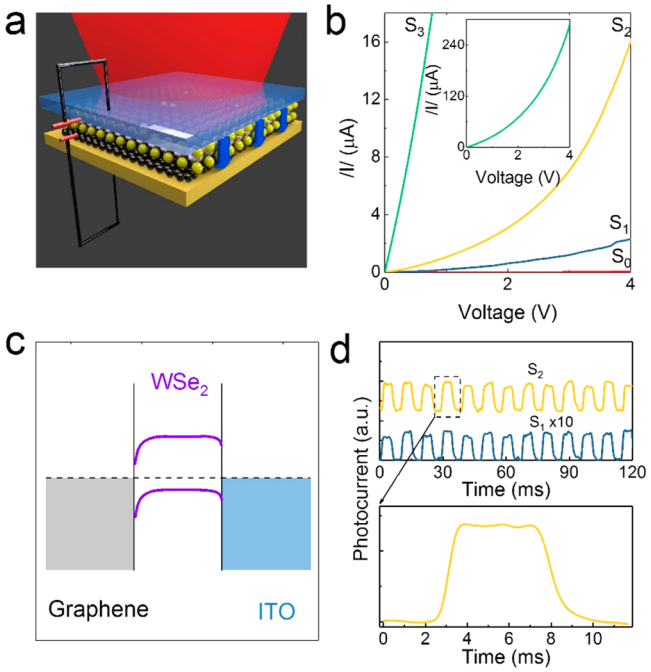


**Figure 4. (a) Experimental setup for the measurement of the interlayer photocurrent of the W/G heterostructure. (b) Transfer characteristics of the as-prepared W/G ($S_0$) photodiode. (c) Corresponding energy band diagram of the $S_0$ photodiode. (d) Time-resolved photoresponse of the photodiode based on $S_1$ and $S_2$.**

by 4 orders of magnitude in $S_3$ as the atomic ratio of Se/W continuously decreased.

The enhanced out-of-plane charge transport *via* point defects provides an efficient method for optimizing or designing photoelectric devices. Here, we present a W/G photodetector with the controlled formation of Se point defects. Figure 5a shows the structure of the photodetector based on the W/G heterostructure, in which graphene and $WSe_2$ monolayers are successively stacked on top of the electrodes. Se point defects with controllable density were fabricated on the $WSe_2$ layer using Ga ion implantation. Figure 5b shows the dark current in the W/G heterostructure as the atomic ratio of Se/W decreased from 1.99 ($S_0$) to 1.75 ($S_3$), where the dark current decreased from 44.68 to 25.91 mA at a voltage of 0.5 V. We believe the decreased dark current is induced by blocked in-plane charge transport in the $WSe_2$ monolayer. The structure of the W/G photodetector is similar to a circuit where graphene and a $WSe_2$ monolayer are connected in parallel. The blocked charge transport in the $WSe_2$ plane increased the total resistance of the parallel circuit. As a result, the dark current decreased after irradiation.

We probe the photoresponse of the W/G photodetector with probe light at 532 nm. Figure 5c shows the photoresponse of photodetectors during illumination with a 532 nm laser at a power ($P$) of 3 mW and voltage of 0.5 V. Switching between on and off states can be observed as the probe light is turned on and off. In the as-prepared W/G photodetectors ($S_0$), the photocurrent was steady at 2.7 $\mu$A. After ion irradiation, the photocurrent increased to 7.6 $\mu$A ($S_1$), 25.7 $\mu$A ($S_2$), and 100.4 $\mu$A ($S_3$). The $I-V$ curves from the W/G photodetectors (Figure 5d) indicate the photocurrent is effectively enhanced after irradiation with Ga ions. Figure 5e shows the calculated photoresponsivity ($R$) of the W/G photodetectors. $S_0$, $S_1$, $S_2$, and $S_3$ have the maximum values of $3.7 \times 10$, $1.2 \times 10^2$, $4.2 \times 10^2$, and $2.1 \times 10^3$ mA/W with $P$ = 0.01 mW, respectively. Obviously, the $R$ value of the modified W/G photodetector ($S_3$) is 2 orders of magnitude larger than that of the pristine photodetector.

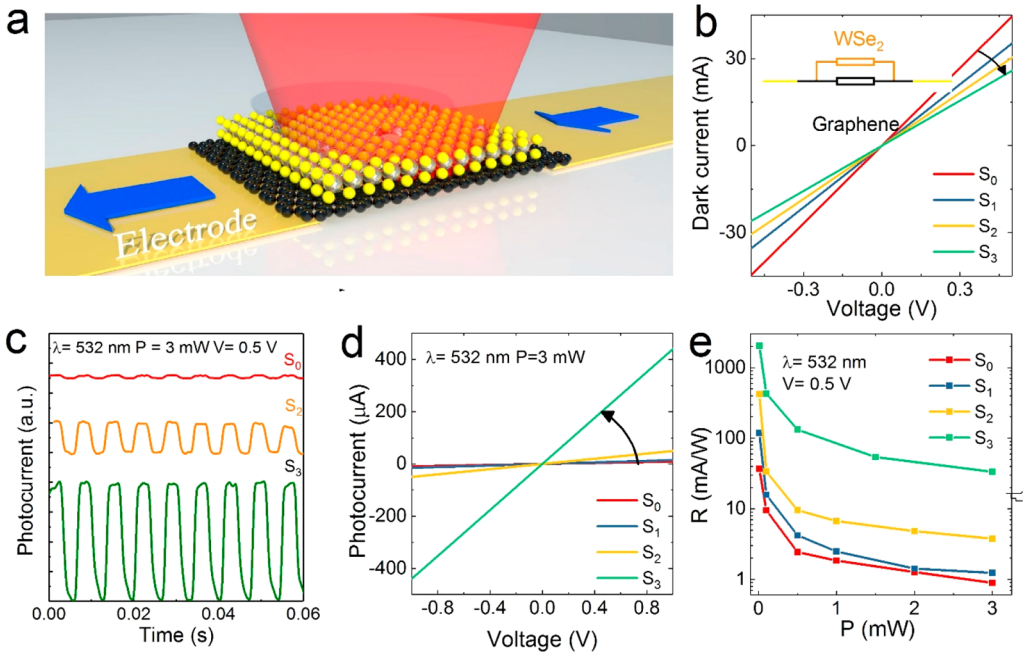


**Figure 5. (a) Schematic diagram of the W/G photodetector. (b) Dark current of the photodetector based on $S_0$, $S_1$, $S_2$, and $S_3$. (c) Time-resolved photoresponse of the photodetectors based on $S_0$, $S_1$, $S_2$, and $S_3$, recorded for probe power of 3 mW, wavelength of 532 nm, and voltage of 0.5 V. (d) $I-V$ curves of the photodetector are based on different W/G heterostructures ($S_0$, $S_1$, $S_2$, and $S_3$). (e) Photoresponsivity of the W/G photodetectors as a function of the probe power.**



DOI: 10.1021/acsnano.8b06503
*ACS Nano* 2018, 12, 10529−10536

We further measured the optical response of the heterostructure device during illumination with near-infrared (NIR) light at 1064 nm. Figure 6a shows the photocurrent

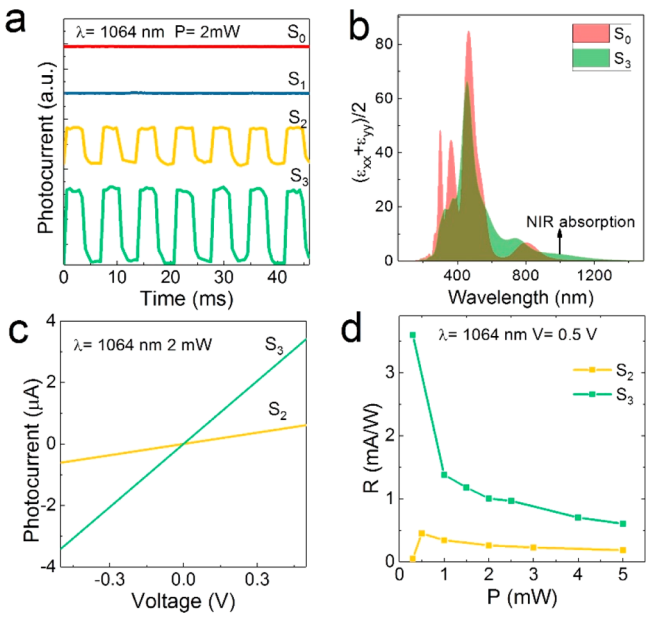


**Figure 6. (a) Time-resolved photoresponse of the photodetectors based on $S_0$, $S_1$, $S_2$, and $S_3$, illuminated by the laser at the wavelength of 1064 nm. (b) Imaginary part of the isotropic dielectric function of $S_0$ and $S_3$. Photocurrent (c) and photoresponsivity (d) of $S_2$ and $S_3$, with the voltage of 0.5 V.**

from the W/G photodetector with probe power of 2 mW and a voltage of 0.5 V. No photoelectric response was observed from $S_0$ because the band gap of pristine $WSe_2$ (1.597 eV) is much larger than the energy of the probe light (1.165 eV), leading to little absorption at 1064 nm. Although graphene has a photoresponse in the NIR regime,[32] the photocurrent is too weak to be observed under the same experimental conditions. When the irradiation time was more than 4 s ($S_2$, $S_3$), a clear photocurrent was observed, which indicates the photoelectric response range of the W/G photodetector expanded from visible to NIR wavelengths due to Ga ion irradiation. The expanded photoresponse can be explained by the formation of intermediate states in $WSe_2$. As shown in Figure 3c, Se point defects generate intermediate states in the forbidden band, thus decreasing the band gap to 1.037 eV, which is less than the energy of the 1064 nm laser. The decreased band gap in $WSe_2$ allows absorption of NIR light, resulting in a photoelectric response during NIR illumination (Figure 6b). We find that the photoresponse due to NIR illumination can be tailored by selecting the appropriate Ga ion dose. As shown in Figure 6c, the maximum photocurrent (2 mW probe power) increased from 0.609 to 2.010 $\mu$A as the irradiation time varied from 4 s ($S_2$) to 8 s ($S_3$). The maximum $R$ value of $S_3$ is 3.6 mA/W, which is much larger than the $R$ value (0.45 mA/W) of $S_2$ (Figure 6d).

To further demonstrate the advantages of the irradiated W/G photodetector, we compared $S_3$ with the photodetectors based on graphene, a $WSe_2$ monolayer, and pristine heterostructures. As shown in Table 1, the highest photoresponsivity of $S_3$ in the visible region (532 nm) was determined to be about 2056 mA/W with an excitation power of 10 $\mu$W, which is $5 \times 10^4$ times larger than that of

**Table 1**

| | $\lambda$ (nm)[a] | $R$ (mA/W) | $I_n$ ($\mu$A) | $V_{ds}$ (V) | $P$ (mW)[b] |
|---|---|---|---|---|---|
| W/G ($S_3$) | 532 | 2056 | 20.56 | 0.5 | 0.01 |
| | 1064 | 1.06 | 0.319 | 0.5 | 0.3 |
| W/G ($S_0$) | 532 | 37 | 0.37 | 0.5 | 0.01 |
| | 1064 | 0 | 0 | 0.5 | <3 |
| $WSe_2$ (CVD) | 532 | 0.04 | 0.004 | 1 | 0.1 |
| | 1064 | 0 | 0 | 1 | <3 |
| graphene (CVD) | 532 | 0 | 0 | 1 | <3 |
| | 1064 | 0 | 0 | 1 | <3 |

[a]The dimension of photosensitive areas is 1 mm × 0.9 mm. [b]$P$ is the power of the detecting laser.

devices based on a pure $WSe_2$ monolayer. In the NIR region (1064 nm), the photoresponsivity of $S_3$ is more sensitive compared to that of pristine graphene, $WSe_2$, and W/G with less than 3 mW excitation power.

## CONCLUSIONS

In this work, we show that point defects enhance out-of-plane charge transport in a vertical W/G heterostructure. Se point defects were artificially generated on the top atomic layer of $WSe_2$ *via* Ga ion irradiation. Based on the probe–pump measurements and numerical fitting, we find that quantity/transfer rate of transferred charges increased by more than a factor of 30/1.6 (Figure 2e). We successfully fabricated a W/G photodetector modified by Se point defects. Our work expands the photoresponse range and the optimized photoresponsivity, which is 2 orders of magnitude larger than the pristine heterostructure (Figure 5f). We compared the modified W/G photodetector with other reported photodetectors based on graphene, $WSe_2$, and pristine heterostructures, and the modified W/G heterostructure exhibits the best photoelectric performance. Our work shows that artificial formation of point defects is an efficient method for optimizing the photoelectric performance of a vertical heterostructure.

## METHODS

**Sample Preparation.** $WSe_2$ monolayers and graphene were produced by CVD on $Al_2O_3$ and copper wafers with a dimension of 10 mm × 10 mm. The heterostructure was constituted by stacking graphene and $WSe_2$ together *via* the wet-chemistry transfer process.

**Ga Ion Irradiation.** The samples were irradiated by the focused $Ga^+$ ion beam facility (model FEI START 400S). The acceleration voltage is 30 kV; the beam current is 93 pA, and the scanning dose is 25.4 nC/$\mu m^2$/s.

**DFT Calculations.** The electron–ion interaction is described by the projector-augmented wave method. The energy cutoff of the plane waves is set to 450 eV with an energy precision of $10^{-5}$ eV. The electron exchange-correlation function is treated using a generalized gradient approximation in the form proposed by Perdew, Burke, and Ernzerhof. The Monkhorst–Pack $k$-point meshes for the Brillouin zone sampling used in structural optimization and electronic structure calculations are 3 × 3 × 1 and 5 × 5 × 1, respectively. A vacuum region up to 15 Å is applied to exclude the interaction between adjacent images. Both atomic positions are fully optimized using the conjugate gradient algorithm until the maximum atomic forces are less than 0.001 eV/Å.

## ASSOCIATED CONTENT

### Supporting Information

The Supporting Information is available free of charge on the ACS Publications website at DOI: 10.1021/acsnano.8b06503.



DOI: 10.1021/acsnano.8b06503
ACS Nano 2018, 12, 10529–10536

Dynamics of the electron-transfer process in $WSe_2$; optical pump−probe measurements; specific detection of out-of-plane charge transport; configuration of the photodetector based on W/G heterostructures; photoresponse of the photodetector based on the $WSe_2$ monolayer; photoresponse of the photodetector based on the graphene monolayer; and secondary electron imaging of the W/G heterostructure (PDF)

## AUTHOR INFORMATION


### Corresponding Authors

*E-mail: tanyang@sdu.edu.cn.
*E-mail: drfchen@sdu.edu.cn.

### ORCID

Yang Tan: 0000-0001-7912-1742
Feng Chen: 0000-0002-9277-9810


### Author Contributions

This paper was written through contributions of all authors. Y.T. provided the original idea and is responsible for the organization and supervision of this work.

### Notes

The authors declare no competing financial interest.

## ACKNOWLEDGMENTS

This work is supported by the National Natural Science Foundation of China (Nos. 11535008 and 11775136). Y.T. acknowledges the financial support from Young Scholars Program of Shandong University (No. 2015WLJH20).

## REFERENCES


(1) Wang, X.; Xia, F. Van der Waals heterostructures: Stacked 2D Materials Shed Light. *Nat. Mater.* **2015**, *14*, 264.

(2) Zhang, W. J.; Wang, Q. X.; Chen, Y.; Wang, Z.; Wee, A. T. S. Van der Waals Stacked 2D Layered Materials for Optoelectronics. *2D Mater.* **2016**, *3*, 022001.

(3) Hong, X. P.; Kim, J.; Shi, S. F.; Zhang, Y.; Jin, C. H.; Sun, Y. H.; Tongay, S.; Wu, J. Q.; Zhang, Y. F.; Wang, F. Ultrafast Charge Transfer in Atomically Thin $MoS_2/WS_2$ Heterostructures. *Nat. Nanotechnol.* **2014**, *9*, 682−686.

(4) Liu, Y.; Weiss, N. O.; Duan, X.; Cheng, H. C.; Huang, Y.; Duan, X. F. Van der Waals Heterostructures and Devices. *Nat. Rev. Mater.* **2016**, *1*, 16042.

(5) Wang, H.; Liu, F.; Fu, W.; Fang, Z.; Zhou, W.; Liu, Z. Two-dimensional Heterostructures: Fabrication, Characterization, and Application. *Nanoscale* **2014**, *6*, 12250−12272.

(6) Song, Z. B.; Schultz, T.; Ding, Z. J.; Lei, B.; Han, C.; Amsalem, P.; Lin, T. T.; Chi, D. Z.; Wong, S. L.; Zheng, Y. J.; Li, M. Y.; Li, L. J.; Chen, W.; Koch, N.; Huang, Y. L.; Wee, A. T. S. Electronic Properties of a 1D Intrinsic/p-Doped Heterojunction in a 2D Transition Metal Dichalcogenide Semiconductor. *ACS Nano* **2017**, *11*, 9128−9135.

(7) Gong, Y.; Lin, J.; Wang, X.; Shi, G.; Lei, S.; Lin, Z.; Zou, X.; Ye, G.; Vajtai, R.; Yakobson, B. I.; Terrones, H.; Terrones, M.; Tay, B. K.; Lou, J.; Pantelides, S. T.; Liu, Z.; Zhou, W.; Ajayan, P. M. Vertical and In-plane Heterostructures from $WS_2/MoS_2$ Monolayers. *Nat. Mater.* **2014**, *13*, 1135.

(8) Liu, Z.; Ma, L.; Shi, G.; Zhou, W.; Gong, Y.; Lei, S.; Yang, X.; Zhang, J.; Yu, J.; Hackenberg, K. P.; Babakhani, A.; Idrobo, J. C.; Vajtai, R.; Lou, J.; Ajayan, P. M. In-plane Heterostructures of Graphene and Hexagonal Boron Nitride with Controlled Domain Sizes. *Nat. Nanotechnol.* **2013**, *8*, 119.

(9) Liu, Y.; Shivananju, B. N.; Wang, Y. S.; Zhang, Y. P.; Yu, W. Z.; Xiao, S.; Sun, T.; Ma, W. L.; Mu, H. R.; Lin, S. H.; Zhang, H.; Lu, Y. R.; Qiu, C. W.; Li, S. J.; Bao, Q. Highly Efficient and Air Stable Infrared Photodetector Based on 2D Layered Graphene-Black Phosphorus Heterostructure. *ACS Appl. Mater. Interfaces* **2017**, *9*, 36137−36145.

(10) Bao, Q. L.; Loh, K. P. Graphene Photonics, Plasmonics, and Broadband Optoelectronic Devices. *ACS Nano* **2012**, *6*, 3677−3694.

(11) Huang, Y. L.; Ding, Z. J.; Zhang, W. J.; Chang, Y. H.; Shi, Y. M.; Li, L. J.; Song, Z. B.; Zheng, Y. J.; Chi, D. Z.; Quek, S. Y.; Wee, A. T. S. Gap States at Low-Angle Grain Boundaries in Monolayer Tungsten Diselenide. *Nano Lett.* **2016**, *16*, 3682−3688.

(12) Qi, D. Y.; Wang, Q. X.; Han, C.; Jiang, J. Z.; Zheng, Y. J.; Chen, W.; Zhang, W. J.; Wee, A. T. S. Reducing the Schottky Barrier Between Few-Layer $MoTe_2$ and Gold. *2D Mater.* **2017**, *4*, 045016.

(13) Wang, Z.; Dong, Z. G.; Gu, Y. H.; Chang, Y. H.; Zhang, L.; Li, L. J.; Zhao, W. J.; Eda, G.; Zhang, W. J.; Grinblat, G.; Maier, S. A.; Yang, J. K. W.; Qiu, C. W.; Wee, A. T. S. Giant Photoluminescence Enhancement in Tungsten-Diselenide-Gold Plasmonic Hybrid Structures. *Nat. Commun.* **2016**, *7*, 11283.

(14) Zhang, W. J.; Chiu, M. H.; Chen, C. H.; Chen, W.; Li, L. J.; Wee, A. T. S. Role of Metal Contacts in High-Performance Phototransistors Based on $WSe_2$ Monolayers. *ACS Nano* **2014**, *8*, 8653−8661.

(15) Zhou, W.; Zou, X.; Najmaei, S.; Liu, Z.; Shi, Y.; Kong, J.; Lou, J.; Ajayan, P. M.; Yakobson, B. I.; Idrobo, J. C. Intrinsic Structural Defects in Monolayer Molybdenum Disulfide. *Nano Lett.* **2013**, *13*, 2615−2622.

(16) Yazyev, O. V.; Chen, Y. P. Polycrystalline Graphene and Other Two-Dimensional Materials. *Nat. Nanotechnol.* **2014**, *9*, 755−767.

(17) Suh, J.; Park, T. E.; Lin, D. Y.; Fu, D.; Park, J.; Jung, H. J.; Chen, Y.; Ko, C.; Jang, C.; Sun, Y.; Sinclair, R.; Chang, J.; Tongay, S.; Wu, J. Doping Against the Native Propensity of $MoS_2$: Degenerate Hole Doping by Cation Substitution. *Nano Lett.* **2014**, *14*, 6976−6982.

(18) Yuan, J.; Najmaei, S.; Zhang, Z.; Zhang, J.; Lei, S.; Ajayan, P. M.; Yakobson, B. I.; Lou, J. Photoluminescence Quenching and Charge Transfer in Artificial Heterostacks of Monolayer Transition Metal Dichalcogenides and Few-layer Black Phosphorus. *ACS Nano* **2015**, *9*, 555−563.

(19) Sreeprasad, T. S.; Nguyen, P.; Kim, N.; Berry, V. Controlled, Defect-guided, Metal-nanoparticle Incorporation onto $MoS_2$ *via* Chemical and Microwave Routes: Electrical, Thermal, and Structural Properties. *Nano Lett.* **2013**, *13*, 4434−4441.

(20) Bertoni, R.; Nicholson, C. W.; Waldecker, L.; Hübener, H.; Monney, C.; De Giovannini, U.; Puppin, M.; Hoesch, M.; Springate, E.; Chapman, R. T.; Cacho, C.; Wolf, M.; Rubio, A.; Ernstorfer, R. Generation and Evolution of Spin-valley, and Layer-Polarized Excited Carriers in Inversion-Symmetric $WSe_2$. *Phys. Rev. Lett.* **2016**, *117*, 277201.

(21) Volmer, F.; Pissinger, S.; Ersfeld, M.; Kuhlen, S.; Stampfer, C.; Beschoten, B. Intervalley Dark Trion States with Spin Lifetimes of 150 ns in $WSe_2$. *Phys. Rev. B: Condens. Matter Mater. Phys.* **2017**, *95*, 235408.

(22) Borzda, T.; Gadermaier, C.; Vujicic, N.; Topolovsek, P.; Borovsak, M.; Mertelj, T.; Viola, D.; Manzoni, C.; Pogna, E. A. A.; Brida, D.; Antognazza, M. R.; Scotognella, F.; Lanzani, G.; Cerullo, G.; Mihailovic, D. Charge Photogeneration in Few-Layer $MoS_2$. *Adv. Funct. Mater.* **2015**, *25*, 3351−3358.

(23) Chen, L.; Li, B.; Zhang, C.; Huang, X.; Wang, X.; Xiao, M. Composition-Dependent Energy Splitting between Bright and Dark Excitons in Lead Halide Perovskite Nanocrystals. *Nano Lett.* **2018**, *18*, 2074−2080.

(24) Li, W.; Zhang, C.; Liu, S.; Ding, X.; Wu, X.; Wang, X.; Wen, H.; Xiao, M. Mott behavior in $K_xFe_{2-y}Se_2$ Superconductors Studied by Pump-probe Spectroscopy. *Phys. Rev. B: Condens. Matter Mater. Phys.* **2014**, *89*, 134515.

(25) Xia, F.; Mueller, T.; Lin, Y.; Valdes-Garcia, A.; Avouris, P. Ultrafast Graphene Photodetector. *Nat. Nanotechnol.* **2009**, *4*, 839.

(26) George, P. A.; Strait, J.; Dawlaty, J.; Shivaraman, S.; Chandrashekhar, M.; Rana, F.; Spencer, M. G. Ultrafast Optical-Pump Terahertz-probe Spectroscopy of the Carrier Relaxation and




DOI: 10.1021/acsnano.8b06503
*ACS Nano* 2018, 12, 10529−10536

Recombination Dynamics in Epitaxial Graphene. *Nano Lett.* **2008**, *8*, 4248−4251.
(27) Tongay, S.; Fan, W.; Kang, J.; Park, J.; Koldemir, U.; Suh, J.; Narang, D. S.; Liu, K.; Ji, J.; Li, J.; Sinclair, R.; Wu, J. Tuning Interlayer Coupling in Large-Area Heterostructures with CVD-grown $MoS_2$ and $WS_2$ Monolayers. *Nano Lett.* **2014**, *14*, 3185−3190.
(28) Fang, H.; Battaglia, C.; Carraro, C.; Nemsak, S.; Ozdol, B.; Kang, J. S.; Bechtel, H. A.; Desai, S. B.; Kronast, F.; Unal, A. A.; Conti, G.; Conlon, C.; Palsson, G. K.; Martin, M. C.; Minor, A. M.; Fadley, C. S.; Yablonovitch, E.; Maboudian, R.; Javey, A. Strong Interlayer Coupling in Van der Waals Heterostructures Built from Single-Layer Chalcogenides. *Proc. Natl. Acad. Sci. U. S. A.* **2014**, *111*, 6198−6202.
(29) Vega-Mayoral, V.; et al. Exciton and Charge Carrier Dynamics in Few-layer $WS_2$. *Nanoscale* **2016**, *8*, 5428−5434.
(30) Cabanillas-Gonzalez, J.; Grancini, G.; Lanzani, G. Pump-Probe Spectroscopy in Organic Semiconductors: Monitoring Fundamental Processes of Relevance in Optoelectronics. *Adv. Mater.* **2011**, *23*, 5468−5485.
(31) Borzda, T.; Gadermaier, C.; Vujicic, N.; Topolovsek, P.; Borovsak, M.; Mertelj, T.; Viola, D.; Manzoni, C.; Pogna, E. A. A.; Brida, D.; Antognazza, M. R.; Scotognella, F.; Lanzani, G.; Cerullo, G.; Mihailovic, D. Charge Photogeneration in Few-Layer $MoS_2$. *Adv. Funct. Mater.* **2015**, *25*, 3351−3358.
(32) Zhang, Y.; Liu, T.; Meng, B.; Li, X.; Liang, G.; Hu, X.; Wang, Q. Broadband High Photoresponse from Pure Monolayer Graphene Photodetector. *Nat. Commun.* **2013**, *4*, 1811.



DOI: 10.1021/acsnano.8b06503
*ACS Nano* 2018, 12, 10529−10536